PCCP

Can Glycine Betaine Denature Proteins?

Journal:	*Physical Chemistry Chemical Physics*
Manuscript ID	CP-ART-01-2020-000397.R1
Article Type:	Paper
Date Submitted by the Author:	23-Mar-2020

Complete List of Authors:	Acharyya, Arusha; University of Pennsylvania, Department of Chemistry Shin, Dayoung; University of Pennsylvania, Chemistry Troxler, Thomas; University of Pennsylvania, Chemistry Gai, Feng; University of Pennsylvania, Chemistry

Can Glycine Betaine Denature Proteins?

Arusha Acharyya, Dayoung Shin, Thomas Troxler, and Feng Gai*

Department of Chemistry, University of Pennsylvania, Philadelphia, Pennsylvania 19104, United States

*To whom correspondence should be addressed, Email: gai@sas.upenn.edu

Feng Gai
Department of Chemistry
University of Pennsylvania
231 South 34th Street
Philadelphia, PA 19104
USA

ABSTRACT: Glycine betaine (GB) is a naturally occurring osmolyte that has been widely recognized as a protein protectant. Since GB consists of a methylated ammonium moiety, it can engage in strong cation-π interactions with aromatic amino acid sidechains. We hypothesize that such specific binding interactions would allow GB to decrease the stability of proteins that are predominantly stabilized by a cluster of aromatic amino acids. To test this hypothesis, we investigate the effect of GB on the stability of two β-hairpins (or mini-proteins) that contain such a cluster. We find that for both systems the stability of the folded state first decreases and then increases with increasing GB concentration. Such non-monotonic dependence not only confirms that GB can act as a protein denaturant, but also underscores the complex interplay between GB's stabilizing and destabilizing forces toward a given protein. While stabilizing osmolytes all have the tendency to be excluded from the protein surface which is the action underlying their stabilizing effect, our results suggest that in order to quantitatively assess the effect of GB on the stability of any given protein, specific cation-π binding interactions need to be explicitly considered. Moreover, our results show, consistent with other studies, that cation methylation can strengthen the respective cation-π interactions. Taken together, these findings provide new insight into the mechanism by which amino acid-based osmolytes interact with proteins.

Introduction

Glycine betaine (GB) or N,N,N-trimethyl glycine (Figure 1) is a naturally-occurring osmolyte, responsible for maintaining osmosis of environmentally stressed cells by retaining intracellular water and cytoplasmic volume and diluting cellular biopolymers.[1–4] Additionally, like other osmoprotectants, such as trimethylamine N-oxide (TMAO), GB can act as a thermoprotectant, stabilizing the native structure of proteins and counteracting the denaturing effect of destabilizing osmolytes (e.g., urea).[1,5–17] For example, it has been shown that GB can effectively increase the thermal melting temperature of various proteins, such as citrate synthase, β-galactosidase, ribonuclease A, and hen egg white lysozyme.[1,15] Following the widely accepted mechanism of action for protein protecting osmolytes, it is generally believed that the ability of GB to protect proteins against thermal denaturation arises from its preferential exclusion from the protein surface.[1,5,7,9,10,18–20] This 'non-direct-interaction' mechanism would exclude the possibility that GB can destabilize proteins, which requires direct and preferential interactions between the osmolyte molecules and protein backbone units and/or sidechains. However, as a molecular cation, it is expected that GB is able to interact with protein aromatic residues, i.e., phenylalanine (Phe), tyrosine (Tyr), and tryptophan (Trp), via cation-π interactions.[21–27] Indeed, the crystallographic study of Schiefner *et al.*[25] on the complex formed between GB and the periplasmic ProX protein revealed that the quaternary ammonium moiety of GB is situated in a rectangular indole box where the ligand binding is stabilized by cation-π interactions. Therefore, we believe that this ability to directly interact with aromatic sidechains makes it possible for GB to destabilize proteins that are rich in aromatic residues but lacking a specific binding site tailored for quaternary ammonium cations.

The strength of a cation-π interaction depends on the chemical identity of the cation and π systems involved, their relative position/orientation, as well as the solvent environment.[21,22] For aromatic sidechains, the indole ring of Trp has been shown to be a more favorable π system for interacting with cations.[21] Whereas for cations, substituted organic ammonium ions (e.g., $R–NH_3^+$ and $R\text{-}N^+(CH_3)_3$) are frequently found to be involved in cation-π interactions in proteins.[21–23,25,26] For example, binding of the neurotransmitter acetylcholine (ACh) to nicotinic acetylcholine receptor proteins is promoted by a cation-π interaction involving a Trp residue on the protein and the trimethylammonium cationic moiety of ACh.[28–31] Similarly, this type of interactions is found to play a critical role in recognizing post-translational modifications of histone and chromatin proteins where the positively charged ε-amino groups of lysine (Lys) residues are methylated to interact with aromatic cages consisting of two or four aromatic residues.[32,33] Moreover, Waters *et al*. have shown that each consecutive N-methylation on a Lys sidechain enhances the magnitude of its cation-π interaction with a Trp residue in a peptide environment.[26] Based on these studies, we hypothesize that GB can act as a denaturant toward proteins that are stabilized by aromatic residues, especially Trp, and its denaturing efficiency is higher than that of the less methylated analogues. To validate this hypothesis, we studied the effect of glycine (Gly), N,N-dimethylglycine (DMG), and GB (Figure 1) on (1) the hydration status of an indole analog, 7-cyanoindole (7-CNI), and (2) the thermal stability of a mutant of the Trpzip5 β-hairpin[34,35] wherein the two native Trp amino acids are replaced by 5-cyanotryptoan (5CN-Trp) (the corresponding mutant is hereinafter referred to as 5CN-Trpzip5) and a mutant of the Trpzip2 β-hairpin[34,35] wherein the four native Trp amino acids are replaced by 5CN-Trp (the corresponding mutant is hereinafter referred to as 5CN-Trpzip2).

The first study is aimed to determine whether these cationic molecules can directly interact with the indole (or indole-like) ring. The reason that we use 7-CNI instead of indole is based on a recent study by Mukherjee *et al*.[36] which demonstrated that the fluorescence of 7-CNI is much more sensitive to the local hydration status than that of indole. As shown (Figure 2), GB absorbs strongly in the far-UV region (190–240 nm), thus preventing the application of circular dichroism (CD) spectroscopy to quantitatively assess GB-induced conformational changes of polypeptides composed of only native amino acids (especially when high concentration of GB is required), whose far-UV CD spectra are typically located in this wavelength range. Therefore, we choose to use 5CN-Trpzip5 and 5CN-Trpzip2 in the second study, since both β-hairpins produce a unique CD signature at wavelengths greater than 240 nm due to exciton coupling between 5CN-Trp residues.[35] Because this CD band is further shifted from the absorption spectrum of GB, it allows us to use CD spectroscopy to conveniently probe the dependence of the thermal stability of those mini-proteins on the concentration of GB, which is necessary to help uncover any complex stabilizing-destabilizing behaviors of this osmolyte. Interestingly, our results show that for both model systems, whose folded β-hairpin conformations are stabilized by a cluster of aromatic residues,[34] GB can exert, simultaneously, two opposite effects on their stability, with one being stabilizing and the other being destabilizing. Since these two effects have different dependences on the GB concentration, the net result is that the β-hairpin stability first decreases and then increases with increasing GB concentration. We believe that this is an important finding as it provides direct evidence showing that GB can act as a protein denaturant and hence offering new insight into the molecular actions of GB.

Experimental details

Materials and sample preparation

All materials were of the highest purity and used as received. Specifically, 7-cyanoindole (99%) was obtained from Ark Pharm Inc., glycine, dimethylglycine and betaine anhydrous were obtained from Fisher Chemicals. 5CN-Trpzip2 (sequence: $SW_{CN}TW_{CN}ENGKW_{CN}TW_{CN}K$, where W_{CN} represents 5CN-Trp) and 5CN-Trpzip5 (sequence: $GEW_{CN}TYDDATKTFTW_{CN}TE$) were synthesized on a microwave-assisted Liberty Blue peptide synthesizer (CEM, Matthews, NC, USA) using Fmoc-protected amino acids purchased from Protein Technologies (Tucson, AZ, USA). Synthesized peptide was further purified by reverse-phase high-performance liquid chromatography (HPLC) and its identity was confirmed by mass spectrometry. Peptide samples were prepared by dissolving an appropriate amount of lyophilized peptide solid in either water (for 5CN-Trpzip2) or pH 7.0 phosphate buffer (for 5CN-Trpzip5) in the presence or absence of the desired osmolyte co-solute. The co-solute concentration was calculated based on mass and solution volume. The peptide concentration was determined optically using the absorbance at 280 nm and a molar extinction coefficient of 5500 M^{-1} cm^{-1} for 5CN-Trp.

Spectroscopic measurements

UV-vis absorption spectra were collected on a Jasco V-650 UV-vis spectrophotometer using a 1.0 cm quartz cuvette at room temperature. CD spectra were measured on a Jasco J-1500 circular dichroism spectrometer using a 1 mm quartz cuvette. All samples used in the CD measurements had a peptide concentration of ca. 50 μM. Fluorescence spectra were collected on a Jobin Yvon Horiba Fluorolog 3.10 fluorometer using a 1.0 cm quartz cuvette at 25 °C and an excitation wavelength of 308 nm. The spectral resolution and scanning rate were set at 1.0 nm and 1 nm/s, respectively. For each 7-CNI sample, a background fluorescence spectrum was collected using

the corresponding co-solute solution only and was subtracted from that of the sample solution. All samples used in the fluorescence spectral measurements had the same 7-CNI concentration (ca. 20 μM). Fourier-transform infrared (FTIR) spectra were collected on a Nicolet Magna-IR 860 spectrometer with 1 cm^{-1} resolution at room temperature. Samples were prepared by dissolving a calculated amount of 7-CNI in either methanol (MeOH) or a 2.0 M GB in MeOH solution, reaching a final concentration of ca. 20 mM. Other details about the sample holder, which consists of two CaF_2 windows separated by a 50 μm spacer, and the FTIR set-up have been described elsewhere.[37]

Global fitting of CD thermal melting curves

To provide a more quantitative estimate of the effect of GB on the thermal stability of a given β-hairpin, we used the following two-state model to globally fit all the CD thermal melting curves:[38]

$$[\theta](T) = \frac{\theta_{\mathrm{U}}(T) + K_{\mathrm{eq}}(T) \cdot \theta_{\mathrm{F}}(T)}{1 + K_{\mathrm{eq}}(T)} \quad (1)$$

$$K_{\mathrm{eq}}(T) = \exp(-\Delta G(T) / RT) \quad (2)$$

$$\Delta G(T) = \Delta H_{\mathrm{m}} + \Delta C_{\mathrm{p}} \cdot (T - T_{\mathrm{m}}) - T \cdot [\Delta S_{\mathrm{m}} + \Delta C_{\mathrm{p}} \cdot \ln(T / T_{\mathrm{m}})] \quad (3)$$

Here, $[\theta](T)$ is the CD signal, $\theta_F(T)$ and $\theta_U(T)$ are the folded and unfolded CD baselines, respectively, $K_{eq}(T)$ is the folding equilibrium constant, $T_m = \Delta H_m/\Delta S_m$ is the thermal melting temperature, ΔH_m is the enthalpy change at T_m, ΔS_m is the entropy change at T_m, and ΔC_p is the heat capacity change. In the current analysis, both $\theta_F(T)$ and $\theta_U(T)$ were assumed to be temperature independent, i.e., $\theta_F(T) = a$ and $\theta_U(T) = b$, where a and b are constants and were treated as global fitting parameters.

Fluorescence lifetime measurements

Fluorescence decay kinetics were measured on a home-built, time-correlated single photon counting (TCSPC) apparatus, the detail of which has been described elsewhere.[39] Briefly, the excitation pulse (270 nm) was generated by frequency tripling of the fundamental output of a femtosecond Ti:Sapphire oscillator. An electro-optical pulse picker (Conoptics, Inc.) was used to decrease the repetition rate of the system to 21 MHz. Fluorescence emission was isolated through a combination of a 355/45 nm bandpass filter and a 300 nm long-pass filter (Semrock) and collected with a MCP-PMT detector (Hamamatsu R2809U) under magic angle polarization condition and digitized by a TCSPC board (Becker and Hickl SPC-730). Fluorescence decay curves were fit to exponential functions using the Fluorofit program (PicoQuant GmbH) and an experimentally determined instrument response function (IRF). All measurements were carried out at room temperature, using a 1.0 cm quartz cuvette and a sample concentration of 20 μM.

Isothermal titration calorimetry (ITC)

A MicroCal iTC200 (Malvern, United Kingdom) was used for the ITC experiment, where the sample cell contained a 100 μM 5CN-Trpzip5 aqueous solution and the injection syringe

contained an aqueous GB (i.e., ligand) stock solution. Unlike common biological ITC measurements where the highest ligand concentration reached at the end of the titration is in the high μM or low mM range, the current case requires a much higher GB concentration. Therefore, to avoid producing a very large ligand dilution heat from each injection, the ITC measurements were divided into six segments; each has a different initial GB concentration. Specifically, for the first three segments a 0.5 M GB stock solution was used and the GB concentration in the sample cell covered the range of 0.05–0.16, 0.16–0.32, and 0.32–0.40 M, respectively. For the next three segments a 1.0 M GB stock solution was used and the GB concentration in the sample cell covered the range of 0.40–0.47, 0.47–0.53, and 0.53–0.60 M, respectively. In addition, for the first group, each segment consisted of 13 injections with an injection volume of 3 μL; whereas for the second group, each segment consisted of 20 injections with an injection volume of 2 μL. All other instrument settings were the same, which were: initial delay 60 sec., spacing 180 sec., filter period 5 sec., measurement temperature at 25 °C, reference power of 6 $\mu cals^{-1}$, and stirring speed of 750 rpm. Furthermore, for each ITC segment, a control experiment where the sample cell contained only buffer (i.e., water) was performed to determine the corresponding heat of ligand (GB) dilution.

Results and Discussions

Effect of co-solutes on the fluorescence property of 7-CNI

To assess whether Gly and its methylated derivatives can associate with indole-based aromatic sidechains, we measured their effect on the fluorescence intensity and lifetime of 7-CNI. The experimental design is based on the premise that such attractive interactions would bring the co-

solute molecules in question toward 7-CNI, thus altering its hydration status and, in turn, its fluorescence property.[36]

As shown (Figure 3), all three co-solutes increase the fluorescence intensity of 7-CNI in a concentration dependent manner. However, in comparison to that of Gly, the effects of DMG and GB are larger. For example, in the presence of 2.5 M Gly, the peak fluorescence intensity of 7-CNI is increased by a factor of 1.5, whereas at the same concentration, DMG and GB increase the fluorescence intensity of 7-CNI by a factor of 1.7 and 3.3, respectively. As the study of Mukherjee *et al*.[36] has demonstrated that dehydration increases the fluorescence quantum yield of 7-CNI, these results suggest that these co-solute molecules can reduce the degree of hydration of 7-CNI, most likely by accumulation near the surface of the fluorophore via cation-π interactions.

To further substantiate this notion, we carried out fluorescence lifetime measurements. As shown (Figure 4), in the absence of any co-solute, the fluorescence decay of 7-CNI in water can be fit by a single-exponential function with a lifetime (τ_F) of 1.9 ns, which is in agreement with the study of Hilaire *et al*.[40] However, in the presence of co-solute molecules, the fluorescence decay becomes slower (Figure 4). For example, the τ_F values of 7-CNI obtained in 2.5 M Gly, DMG and GB solutions are 2.4, 3.5 and 4.2 ns, respectively. Moreover, similar to that observed in the fluorescence intensity measurements, the τ_F of 7-CNI increases with increasing co-solute concentration and GB is the most effective in this regard (Figure 5). Since the fluorescence decay rate of 7-CNI is slower in various organic solvents and mixtures of water-organic solvents,[36,40] as compared to that in water, these results provide additional evidence in support of the aforementioned view that these co-solutes can engage in specific interactions with the aromatic ring of 7-CNI, as such interactions would lead to preferential accumulation of the

co-solute molecules around the fluorophore and hence a reduction of its interaction with water molecules.

Because the C≡N stretching frequency of nitrile-indoles depends on local environment,[40,41] we also employed infrared (IR) spectroscopy to assess the interactions between GB and 7-CNI. Since FTIR measurements require a relatively high solute concentration (mM) and 7-CNI is only sparingly soluble in water, methanol (MeOH) was used in this case. As shown (Figure 6), in MeOH the C≡N stretching vibrational band of 7-CNI consists of a strong peak at 2220 cm^{-1} and two weaker ones at 2232 and 2244 cm^{-1}, respectively. As observed for 4-CNI,[41] these spectral features most likely arise from Fermi resonance. As indicated (Figure 6), addition of GB (2.0 M) leads to appreciable changes in the C≡N band of 7-CNI. First, it undergoes a small but detectable red-shift, indicating that, consistent with the fluorescence result, in the presence of GB the 7-CNI molecules are situated in a more hydrophobic environment.[42] Second, its bandwidth becomes substantially narrower, indicating that the 7-CNI molecules in this case experience a more homogeneous environment. Since cation-π interacting forces are short ranged and are strongly directional, preferential binding of GB molecules to 7-CNI via such interactions is expected to make the local environment of 7-CNI more ordered and, as a result, leading to a decrease in the inhomogeneously broadened bandwidth of the C≡N stretching vibration. Therefore, these IR results corroborate the notion that GB can engage in cation-π interactions with indole and indole-like aromatic rings.

Taken together, the equilibrium and time-resolved spectroscopic data presented above suggest that the strength of the interaction between 7-CNI and these Gly-based co-solutes increases with the degree of ammonium methylation. This trend is consistent with several previous studies indicating that N-methylation of the ammonium moiety facilitates cation-π

interactions, as replacing a hydrogen atom with a methyl group reduces the enthalpic penalty arising from cation dehydration (or desolvation) required for complex formation.[21,24,26] Such favorable hydrophobic desolvation effects have been observed in various systems. For example, this effect has been invoked to explain that (1) the affinity of ammonium-containing ligands towards the aromatic binding pocket of factor Xa, a serine protease protein, increases with methylation of the ligand,[23] (2) stepwise increasing methylation from $MeNH_3^+$ to Me_4N^+ resulted in a trend of increasing affinity for tris-indole based hosts,[43] (3) the strength of the cation–π interaction between a Lys and a Trp in a β-hairpin is increased upon N-methylation of the Lys residue,[24] and (4) the recognition of the neurotransmitter acetylcholine, which carries a quaternary ammonium group, by its receptors consisting of an aromatic amino acid binding pocket.[28,31]

Effect of co-solutes on the thermal stability of 5CN-Trpzip2 and 5CN-Trpzip5

The fluorescence results obtained with 7-CNI provide strong evidence showing that GB can effectively interact with indole-based aromatic amino acids. However, these results alone are insufficient to validate the idea that GB can serve as a protein denaturant (for those rich in aromatic residues). Therefore, to provide further information in support of this point, we employed CD spectroscopy to determine the effect of those Gly derivatives on the thermal stabilities of two β-hairpins, 5CN-Trpzip2 and 5CN-Trpzip5, which correspond to the Trp/5CN-Trp mutants of the well-studied Trpzip2 and Trpzip5 β-hairpins, respectively. We chose these model systems not only because they are folded at room temperature, but also because their folded conformation exhibits a positive and intensive CD band at a wavelength greater than 240 nm (243 and 248 nm for 5CN-Trpzip2 and 5CN-Trpzip5, respectively), arising from exciton

coupling between two adjacent 5CN-Trp sidechains.[35] While the corresponding wild-type Trpzip β-hairpins also give rise to a positive exciton CD band, the peak position of this band is at ca. 230 nm. As indicated (Figure 2), GB has a strong far-UV absorption band peaked at 195 nm. As a result, even for a 1 mM GB solution the sample has appreciable absorbance in the wavelength range of 210 – 240 nm. Therefore, this absorption feature of GB is expected to significantly reduce the transmittance of the sample solution and hence the signal-to-noise ratio of the corresponding CD signal near this wavelength region when GB concentration ([GB]) is high (i.e., hundreds of mM and higher). To alleviate this undesirable influence, we chose to use those Trpzip mutants because their characteristic CD bands are further red-shifted from the GB absorption band. In addition, the intensity of these exciton CD bands is sensitively dependent on the separation distance between the two interacting 5CN-Trp residues, making them useful in monitoring the thermal denaturation process of the β-hairpin conformation.

As expected, the intensity of the exciton CD band of 5CN-Trpzip5 depends on [GB] (Figure 7). Interestingly, however, the intensity first decreases and then increases with increasing [GB]. This non-monotonic dependence indicates that at least two opposite effects are at play, with one being destabilizing and the other being stabilizing, and that these two effects have different dependences on [GB]. To provide a more quantitative assessment of the effect of GB on the thermal stability of the β-hairpin conformation of 5CN-Trpzip5, we carried out further thermal melting measurements by following the CD signal at 248 nm using samples having the same peptide concentration but different GB concentrations. As shown (Figure 8), the amplitudes of the CD thermal melting (T-melting) curves at 5.0 ^{o}C also exhibit a non-monotonic dependence on [GB], thus corroborating the results of the spectral measurements. In order to more quantitatively evaluate the thermal stability of the 5CN-Trpzip5 β-hairpin under different

solution conditions, we used a two-state model to globally fit the CD T-melting curves.[38] Specifically, we assumed that the folded and unfolded CD baselines are independent of [GB] and temperature, hence being treated as global fitting parameters (see experimental section). As indicated (Figure 8), this model can adequately fit all the CD T-melting curves with those thermal melting temperatures listed in Table 1. As expected, the thermal melting temperature (T_m) of 5CN-Trpzip5 also exhibits a non-monotonic dependence on [GB], with a minimum (hereafter referred to as $[GB]_{min}$) occurring at around 0.5–0.6 M (Figure 9). In addition, the T_m value (39.4 ^oC) obtained at [GB] = 0 is comparable to that (42 ^oC) reported for the wild-type Trpzip5,[34] indicating that the 5CN-Trp/Trp mutations slightly affect the thermal stability of the Trpzip β-hairpin and that 5CN-Trpzip5 is a valid model system in the current case.

Next we performed an isothermal titration calorimetry (ITC) experiment, treating 5CN-Trpzip5 and GB as the protein and ligand, respectively. We expect that the heat released upon titrating a GB solution into a 5CN-Trpzip5 solution will show a trend that is different from the commonly observed ITC titration data, which typically exhibit a monotonic dependence on the ligand concentration. This is because not only GB can bind to the 5CN-Trp sidechains in 5CN-Trpzip5, it can also shift the folding-unfolding equilibrium constant of the β-hairpin conformation (Figures 8 and 9). In other words, besides the normal binding event, a conformational transition also contributes to the total heat measured in the ITC experiment. While the former process is always accompanied by a negative enthalpy change (ΔH), the latter one can have either a positive or negative ΔH value depending on whether addition of GB promotes 5CN-Trpzip5 to unfold (positive ΔH), which occurs when $[GB]<[GB]_{min}$, or fold (negative ΔH), which occurs when $[GB]>[GB]_{min}$. Therefore, we predict that the net heat signature obtained from the aforementioned ITC measurement will exhibit a non-monotonic

dependence on [GB]. As shown (Figure 10), the ITC raw data (for each injection the heat arising from GB dilution has been subtracted) indeed show such dependence. Specifically, as the concentration of GB increases, the net amount of heat released upon addition of an aliquot of GB into the peptide solution (100 μM) first decreases and then increases, with a minimum occurring at ca. 0.4–0.5 M concentration of GB. This dependence on [GB] is similar to that observed for the T_m of the 5CN-Trpzip5 β-hairpin (Figure 9), hence providing further evidence in support of the notion that GB can unfold this mini-protein at relatively low concentrations.

GB has been mostly regarded as a protectant osmolyte, which is supposed to only increase protein stability, prevent irreversible aggregation and restore protein activities. Indeed, various protein systems have been shown to become more stable in the presence of GB,[5,15,44] including, for example, ribonuclease A (RNase A), hen egg white lysozyme, bovine serum albumin (BSA), and α-lactalbumin (α-LA). Therefore, in the context of those previous studies the results obtained with 5CN-Trpzip5 seem to be surprising. However, the ability of GB to significantly-destabilize or unfold a mini-protein stabilized predominantly by a cluster of aromatic residues is not unexpected when considering the fact that GB can directly bind to hydrophobic sidechains.[18,45] In fact, it has been suggested that the nonpolar character of GB could allow it to more favorably interact with hydrophobic moieties (comparing to Gly), hence competing with or reducing its protein stabilization effect.[20,46] Indeed, consistent with this line of thought several studies have shown that although addition of GB causes the T_m of the protein in question to increase, the net increase exhibits a nonlinear dependence on [GB] and is maximized at a certain GB concentration.[15,16] While such dependence of T_m on [GB] indicates that GB can exhibit both protein stabilizing and destabilizing properties, it is worth noting that the destabilizing effect observed in those previous studies is much less pronounced and only

observed at very high [GB] (4-5 M), in comparison to that observed in the current study. Furthermore, to the best of our knowledge, our study demonstrates for the first time that the GB can act as a denaturant,[8] causing a significant shift of the folding-unfolding equilibrium of a Trpzip mini-protein towards the unfolded state.

To further validate the conclusions reached above, we measured the effect of GB on the CD spectra of another β-hairpin, 5CN-TrpZip2, which is stabilized by four 5CN-Trp residues. As shown (Figure 11A), the intensity of the 5CN-Trp exciton CD band at 243 nm of this peptide exhibits a similar [GB] dependence as that observed for 5CN-TrpZip5. More specifically, at relatively low concentrations the effect of GB is to decrease the characteristic CD signal, whereas at relatively high concentrations this effect is reversed. As indicated (Figure 11B), while the corresponding CD T-melting curves show consistent [GB] dependence, they do not show the characteristics of a cooperative or two-state folding-unfolding transition. However, if we were to use the aforementioned model to globally fit these T-melting data, we obtained those T_m values listed in Table 1. Although the corresponding fits (Figure 11B) are less quantitative, the results nevertheless corroborate the notion that GB can either destabilize or stabilize the β-hairpin conformation of 5CN-Trpzip2, depending on the concentration.

Finally, we compared the effects of Gly, DMG and GB on the stability of 5CN-Trpzip2. As indicated (Figure 12), at 1.0 M concentration, GB induces a significant decrease in the intensity of the exciton CD band, whereas DMG and Gly have a much smaller effect. Therefore, these findings are consistent not only with the fluorescence results obtained with 7-CNI but also with the notion that methylation of a cation can increase its binding affinity towards an aromatic sidechain via cation-π interactions. Moreover, our results are in agreement with previous studies

demonstrating that cation-π interactions play a key role in the complexation of GB with several proteins,[47,48] where the binding pocket is rich in Trp residues.

Furthermore, it is worth noting that our findings could be tested in future studies by 'tuning' the underlying cation-π interaction strength. Gao and coworkers[49,50] have shown that through ring fluorination one could create unnatural aromatic amino acids, such as pentafluorophenylalanine and difluorotyrosin, that prefer hydrophobic to cation-π interactions. Therefore, one potential model system for this purpose is a Trpzip5 mutant wherein the Trp residue is replaced by a highly fluorinated Trp amino acid. We expect that, if this Trpzip5 mutant can fold and our conclusion is true, GB will have a lesser effect on its β-hairpin stability, compared to 5CN-Trpzip5.

Conclusions

Glycine betaine (GB) has been widely studied, due to its role as an important osmoprotectant in nature. Specifically, many studies have shown that GB (typical at high concentrations) can increase the stability of various proteins, indicating that it is a protein stabilizer. However, because GB can interact favorably with aromatic moieties via cation-π interactions, it is possible that GB can act, under certain concentration conditions, as a denaturant for proteins that are rich in aromatic amino acids. To test this possibility, we investigate the dependence of the thermal melting temperature (T_m) of two Trpzip β-hairpins (5CN-TrpZip5 and 5CN-TrpZip2) on GB concentration ([GB]). We find that the T_m of both systems exhibits a complex and non-monotonic dependence on [GB]. For example, the T_m values of the 5CN-TrpZip5 β-hairpin are ca. 39.4, 21.1, and 36.5 ^oC when [GB] = 0.0, 0.5, and 0.8 M, respectively; and those of the 5CN-TrpZip2 β-hairpin are ca. 56.0, -4.8, and 58.9 ^oC when [GB] = 0.0, 1.0., and 2.0 M, respectively.

Thus, taken together, our results show that for these β-hairpins, which are stabilized mainly by a cluster of aromatic amino acids, GB can exert both stabilizing and destabilizing effects and the net result depends on [GB]. Based on this finding, we believe that the ability of GB to engage in cation-π interactions should be considered explicitly in assessing its effect on the folding-unfolding equilibrium of any protein rich in aromatic residues. Furthermore, consistent with previous studies, our results show that increasing the methylation level of ammonium-based cations can increase the cation-π interaction strength.

ACKNOWLEDGEMENTS

This work is partially supported by a seed grant from the NSF MRSEC program at the University of Pennsylvania (DMR17-2053).

References:

1 T. Caldas, N. Demont-Caulet, A. Ghazi and G. Richarme, *Microbiology*, 1999, **145**, 2543–2548.

2 T. H. H. Chen and N. Murata, *Trends Plant Sci.*, 2008, **13**, 499–505.

3 M. Ashraf and M. R. Foolad, *Environ. Exp. Bot.*, 2007, **59**, 206–216.

4 B. Landfald and A. R. Strom, *J. Bacteriol.*, 1986, **165**, 849–855.

5 A. A. Thoppil, E. Judy and N. Kishore, *J. Chem. Thermodyn.*, 2017, **111**, 115–128.

6 G. S. Ratnaparkhi and R. Varadarajan, *J. Biol. Chem.*, 2001, **276**, 28789–28798.

7 D. J. Felitsky and M. T. Record, *Biochemistry*, 2004, **43**, 9276–9288.

8 P. P. Misra and N. Kishore, *Biopolymers*, 2012, **97**, 933–949.

9 M. Auton, J. Rösgen, M. Sinev, L. M. F. Holthauzen and D. W. Bolen, *Biophys. Chem.*, 2011, **159**, 90–99.

10 E. J. Guinn, L. M. Pegram, M. W. Capp, M. N. Pollock and M. T. Record, *Proc. Natl. Acad. Sci. U. S. A.*, 2011, **108**, 16932–16937.

11 N. Kumar and N. Kishore, *Biophys. Chem.*, 2014, **189**, 16–24.

12 G. Somero, *Physiology*, 1986, **1**, 9–12.

13 J. J. Bedford, J. L. Harper, J. P. Leader, P. H. Yancey and R. A. J. Smith, *Comp. Biochem. Physiol. Part B Biochem. Mol. Biol.*, 1998, **119**, 521–526.

14 L. M. Samuelsson, J. J. Bedford, R. A. J. Smith and J. P. Leader, *Comp. Biochem. Physiol. - A Mol. Integr. Physiol.*, 2005, **141**, 22–28.

15 M. M. Santoro, Y. Liu, S. M. A. Khan, L. X. Hou and D. W. Bolen, *Biochemistry*, 1992, **31**, 5278–5283.

16 S. Knapp, R. Ladenstein and A. Galinski, *Extremophiles*, 1999, **3**, 191–198.

17 S. Bourot, O. Sire, A. Trautwetter, T. Touzé, L. F. Wu, C. Blanco and T. Bernard, *J. Biol. Chem.*, 2000, **275**, 1050–1056.

18 M. W. Capp, L. M. Pegram, R. M. Saecker, M. Kratz, D. Riccardi, T. Wendorff, J. G. Cannon and M. T. Record, *Biochemistry*, 2009, **48**, 10372–10379.

19 D. J. Felitsky, J. G. Cannon, M. W. Capp, J. Hong, A. W. Van Wynsberghe, C. F. Anderson and M. T. Record, *Biochemistry*, 2004, **43**, 14732–14743.

20 T. Arakawa and S. N. Timasheff, *Arch. Biochem. Biophys.*, 1983, **224**, 169–177.

21 E. A. Orabi and G. Lamoureux, *J. Phys. Chem. B*, 2018, **122**, 2251–2260.

22 C. Rapp, E. Goldberger, N. Tishbi and R. Kirshenbaum, *Proteins Struct. Funct. Bioinforma.*, 2014, **82**, 1494–1502.

23 L. M. Salonen, C. Bucher, D. W. Banner, W. Haap, J. L. Mary, J. Benz, O. Kuster, P. Seiler, W. B. Schweizer and F. Diederich, *Angew. Chemie - Int. Ed.*, 2009, **48**, 811–814.

24 R. M. Hughes, M. L. Benshoff and M. L. Waters, *Chem. - A Eur. J.*, 2007, **13**, 5753–5764.

25 A. Schiefner, J. Breed, L. Bösser, S. Kneip, J. Gade, G. Holtmann, K. Diederichs, W. Welte and E. Bremer, *J. Biol. Chem.*, 2004, **279**, 5588–5596.

26 R. M. Hughes and M. L. Waters, *J. Am. Chem. Soc.*, 2005, **127**, 6518–6519.

27 H. M. Khan, A. D. Mackerell. Jr and N. Reuter, *J. Chem. Theory Comput.*, 2018, **15**, 7–12.

28 J. D. Schmitt, C. G. V. Sharples and W. S. Caldwell, *J. Med. Chem.*, 1999, **42**, 3066–3074.

29 X. Xiu, N. L. Puskar, J. A. P. Shanata, H. A. Lester and D. A. Dougherty, *Nature*, 2009, **458**, 534–537.

30 D. L. Beene, G. S. Brandt, W. Zhong, N. M. Zacharias, H. A. Lester and D. A. Dougherty, *Biochemistry*, 2002, **41**, 10262–10269.

31 S. Roelens and R. Torriti, *J. Am. Chem. Soc.*, 1998, **120**, 12443–12452.

32 A. H. F. M. Peters, S. Kubicek, K. Mechtler, R. J. O'Sullivan, A. A. H. A. Derijck, L. Perez-Burgos, A. Kohlmaier, S. Opravil, M. Tachibana, Y. Shinkai, J. H. A. Martens and T. Jenuwein, *Mol. Cell*, 2003, **12**, 1577–1589.

33 R. J. Sims, K. Nishioka and D. Reinberg, *Trends Genet.*, 2003, **19**, 629–639.

34 A. G. Cochran, N. J. Skelton and M. A. Starovasnik, *Proc. Natl. Acad. Sci. U. S. A.*, 2001, **98**, 5578–5583.

35 D. Mukherjee and F. Gai, *Anal. Biochem.*, 2016, **507**, 74–78.

36 D. Mukherjee, L. I. Ortiz Rodriguez, M. R. Hilaire, T. Troxler and F. Gai, *Phys. Chem. Chem. Phys.*, 2018, **20**, 2527–2535.

37 B. Ding, M. R. Hilaire and F. Gai, *J. Phys. Chem. B*, 2016, **120**, 5103−5113.

38 Y. Zhu, J. G. Saven and F. Gai, *Chem. Phys.*, 2004, **307**, 99–109.

39 P. A. Hill, Q. Wei, T. Troxler and I. J. Dmochowski, *J. Am. Chem. Soc.*, 2009, **131**, 3069–3077.

40 M. R. Hilaire, D. Mukherjee, T. Troxler and F. Gai, *Chem. Phys. Lett.*, 2017, **685**, 133–138.

41 J. M. Rodgers, R. M. Abaskharon, B. Ding, J. Chen, W. Zhang and F. Gai, *Phys. Chem. Chem. Phys.*, 2017, **19**, 16144-16150.

42 Z. Getahun, C-Y. Huang, T. Wang, B. De Leon, W. F. DeGrado and F. Gai. *J. Am. Chem. Soc.*, 2003, **125**, 405-411.

43 A. L. Whiting, N. M. Neufeld and F. Hof, *Tetrahedron Lett.*, 2009, **50**, 7035–7037.

44 A. Rani and P. Venkatesu, *Phys. Chem. Chem. Phys.*, 2018, **20**, 20315–20333.

45 Y. L. Shek and T. V Chalikian, *J. Phys. Chem. B*, 2011, **115**, 11481–11489.

46 L. R. Singh, N. K. Poddar, T. A. Dar, R. Kumar and F. Ahmad, *Life Sci.*, 2011, **88**, 117–125.

47 C. Horn1, L. Sohn-Bosser, J. Breed, W. Welte, L. Schmitt and E. Bremer, *J. Mol. Biol.*, 2006, **357**, 592-606.

48 I. Fujisawa and K. Aoki, *Crystals*, 2013, **3**, 306-314.

49 C. J. Pace and J. Gao, *Acc. Chem. Res*., 2013, **46**, 907-915.

50 T. He, A. Gershenson, S. J. Eyles, Y-J Lee, W. R. Liu, J. Wang, J. Gao and M. F. Roberts, *J. Biol. Chem.*, 2015, **290**, 19334-19342.

Table 1. Thermal melting temperature (T_m) values of 5CN-Trpzip5 and 5CN-Trpzip2 at different GB concentrations, obtained by globally fitting the corresponding CD T-melting curves.

[GB] (M)	5CN-Trpzip5: T_m (° C)	[GB] (M)	5CN-Trpzip2: T_m (° C)
0.00	39.4 ± 2.0	0.0	56.0 ± 2.0
0.25	35.2 ± 1.0	1.0	-4.8 ± 2.0
0.35	34.3 ± 1.0	2.0	58.9 ± 2.0
0.40	24.1 ± 2.0		
0.50	21.1 ± 1.0		
0.65	31.6 ± 2.0		
0.80	36.5 ± 1.0		

Figure Captions

Figure 1. Zwitterionic forms of the co-solutes used in the current study.

Figure 2. Absorption spectrum of a 1 mM GB sample in a 1 cm pathlength cuvette.

Figure 3. Normalized fluorescence spectra of 7-CNI obtained in different co-solute solutions, as indicated. In each case, the 7-CNI concentration was maintained at a constant value (ca. 20 μM), whereas the concentrations of the corresponding co-solute were 0.0, 0.5, 1.5, and 2.5 M, respectively. In addition, the fluorescence intensities were normalized with respect to that obtained in 2.5 M co-solute concentration.

Figure 4. Representative fluorescence decay curves of 7-CNI obtained in water and different co-solute (1.0 M) solutions, as indicated. In each case, the black line corresponds to a single-exponential fit to the decay kinetics and the corresponding residuals are given in the top panel. The resultant τ_F values are 1.9, 2.1, 2.6, and 2.7 ns for water, Gly, DMG, GB, respectively.

Figure 5. Dependence of the fluorescence lifetime of 7-CNI on co-solute and co-solute concentration.

Figure 6. Normalized FTIR spectra of 7-CNI in MeOH (blue) and a 2.0 M GB MeOH solution (red), showing the difference in the C ≡ N stretching vibrational bands.

Figure 7. CD spectra of 5CN-Trpzip5 obtained at 4.0 °C and different GB concentrations, as indicated.

Figure 8. Normalized CD T-melting curves of 5CN-Trpzip5 obtained at 248 nm and in phosphate buffer (pH 7.0) solutions of different GB concentrations, as indicated. In each case, the CD intensity was normalized against the CD signal obtained in buffer at 0 °C. The solid black lines are global fits to the two-state model described in the text, and the dashed lines represent the global folded and unfolded CD baselines, respectively.

Figure 9. Dependence of the thermal melting temperature (T_m) of 5CN-Trpzip5 on GB concentration.

Figure 10. ITC heat signature obtained by injecting a GB solution into a 5CN-Trpzip5 solution, where the corresponding heat of dilution has been subtracted. For each segment, the respective change in [GB] is indicated. The smaller positive peaks observed are mostly due to solvent mismatch as the GB concentration in the syringe was relatively high.

Figure 11. (A) CD spectra of 5CN-Trpzip2 obtained at 4.0 °C and at different GB concentrations, as indicated. (B) CD T-melting curves of 5CN-Trpzip2 obtained at 243 nm and at different GB concentrations, as indicated. The solid black lines are global fits to the two-state model described in the text.

Figure 12. CD spectra of 5CN-Trpzip2 at 4 °C, in water and different co-solute (1.0 M) solutions, as indicated.

Figure 1

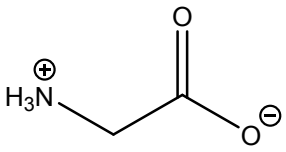

Glycine (Gly)

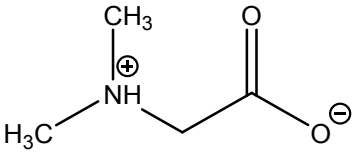

Dimethylglycine (DMG)

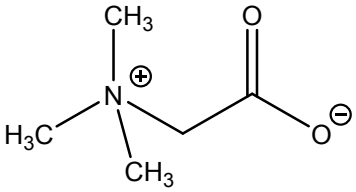

Glycine Betaine (GB)

Figure 2

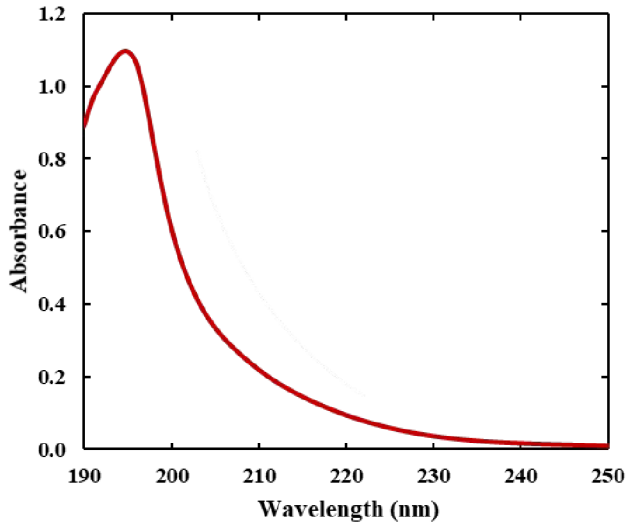
1.2
1.0
0.8
0.6
0.4
0.2
0.0
Absorbance
190
200
210
220
230
240
250
Wavelength (nm)

Figure 3

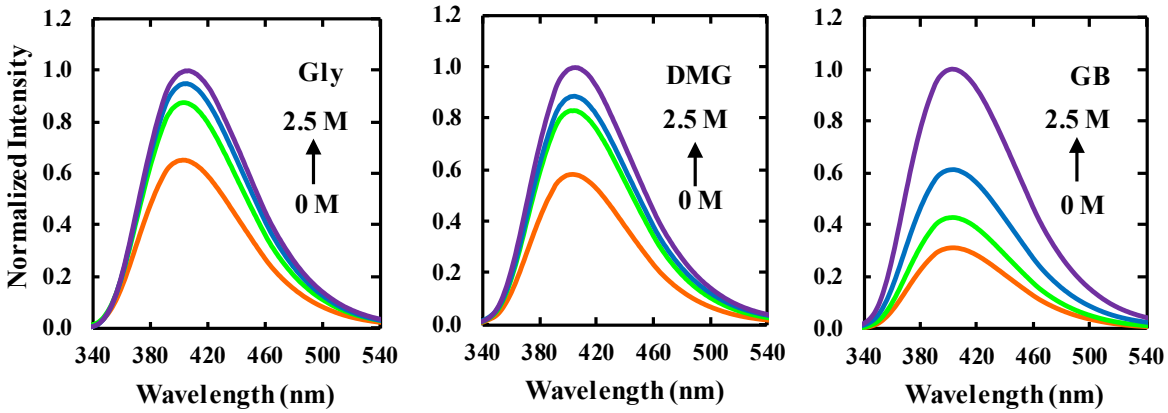
Normalized Intensity
1.2
1.0
0.8
0.6
0.4
0.2
0.0
340 380 420 460 500 540
Wavelength (nm)
Gly
2.5 M
0 M
DMG
2.5 M
0 M
GB
2.5 M
0 M

Figure 4

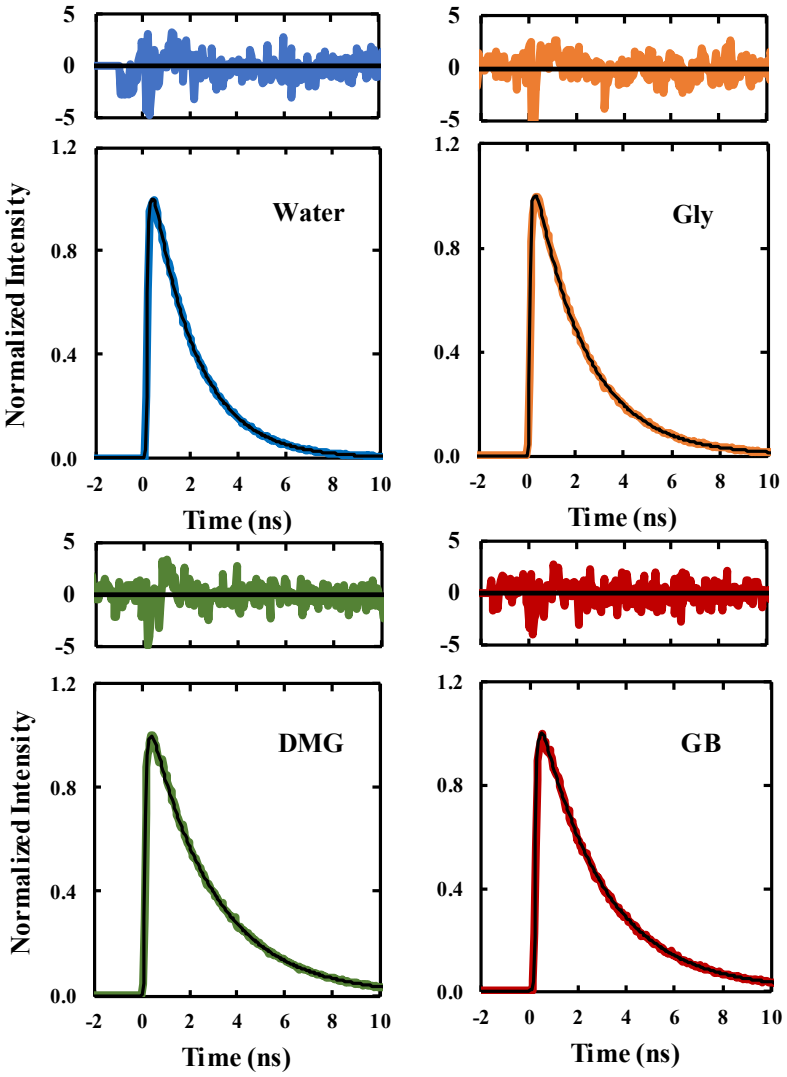

Figure 5

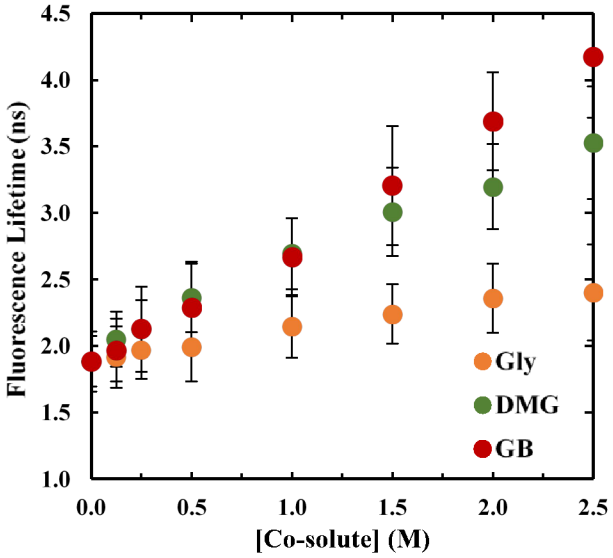
Fluorescence Lifetime (ns)
4.5
4.0
3.5
3.0
2.5
2.0
1.5
1.0
0.0
0.5
1.0
1.5
2.0
2.5
[Co-solute] (M)
Gly
DMG
GB

Figure 6

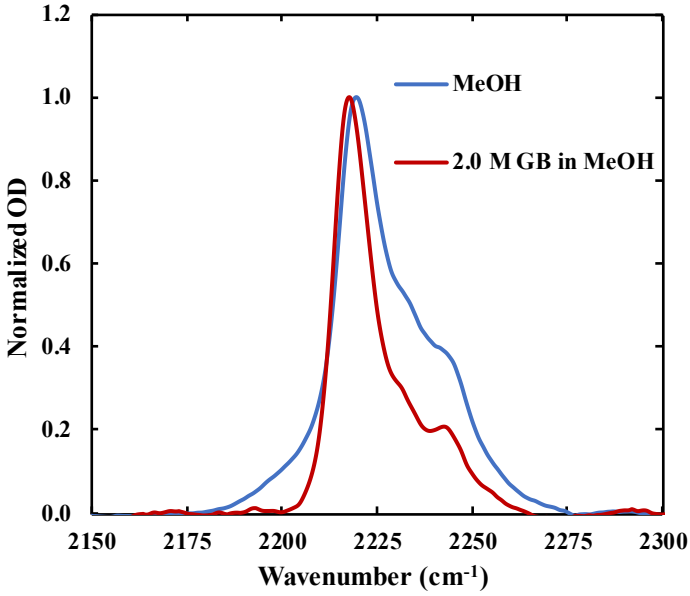
1.2
1.0
0.8
0.6
0.4
0.2
0.0
Normalized OD
2150
2175
2200
2225
2250
2275
2300
Wavenumber (cm-1)
MeOH
2.0 M GB in MeOH

Figure 7

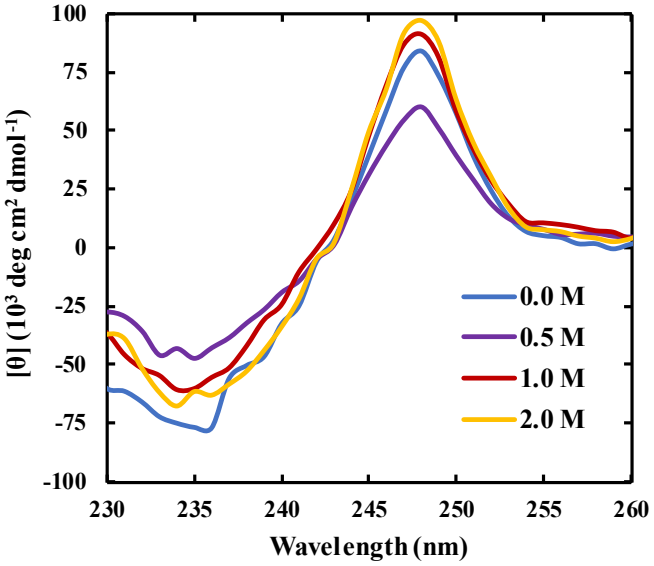
100
75
50
25
0
-25
-50
-75
-100
230
235
240
245
250
255
260
[θ] (10³ deg cm² dmol⁻¹)
Wavelength (nm)
0.0 M
0.5 M
1.0 M
2.0 M

Figure 8

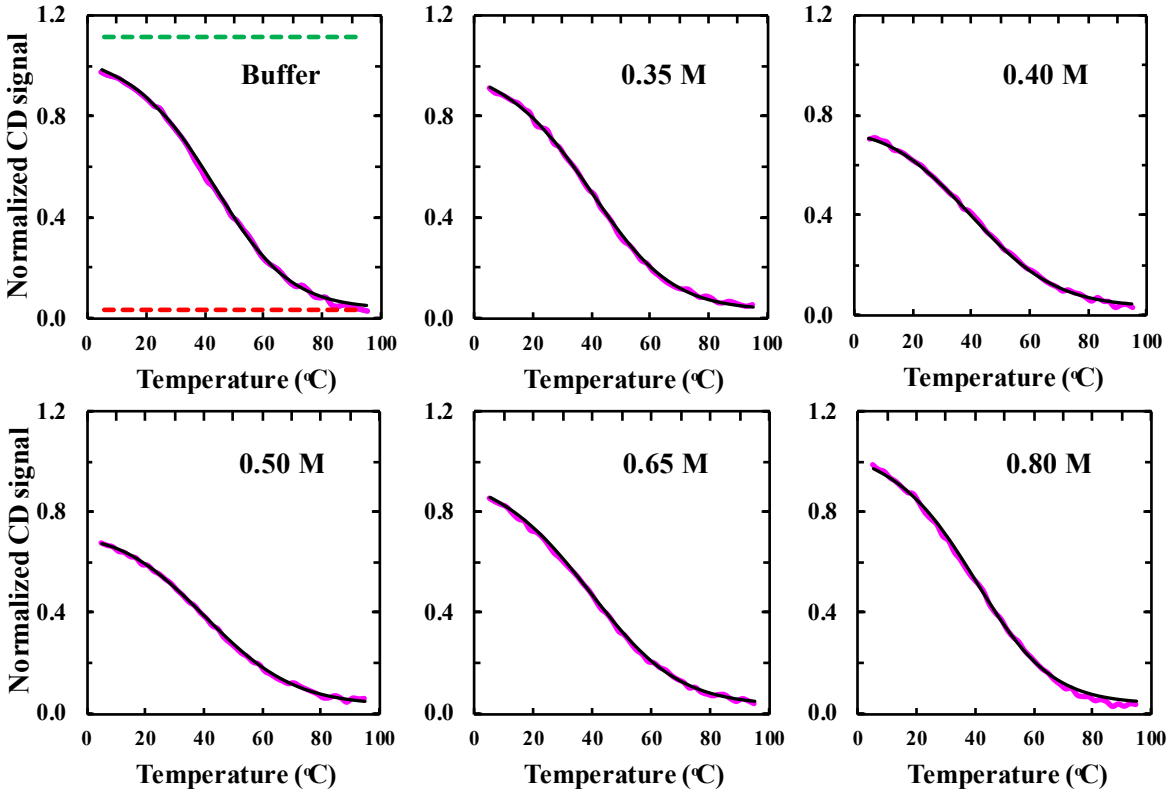
Buffer
0.35 M
0.40 M
0.50 M
0.65 M
0.80 M
Normalized CD signal
Temperature (°C)
0.0
0.4
0.8
1.2
0
20
40
60
80
100

Figure 9

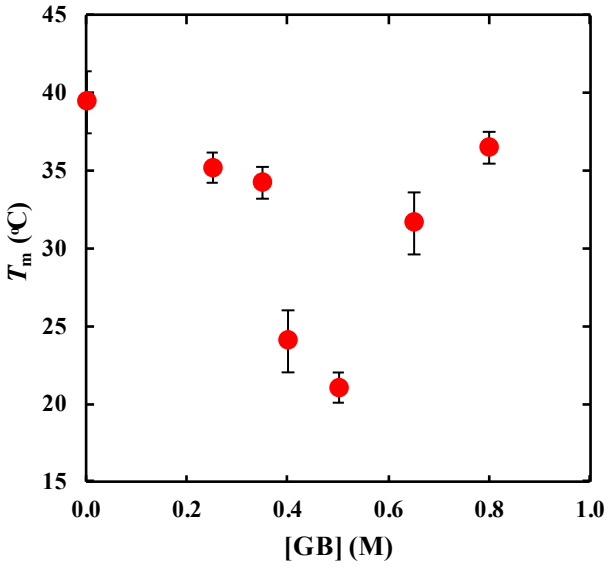

Figure 10

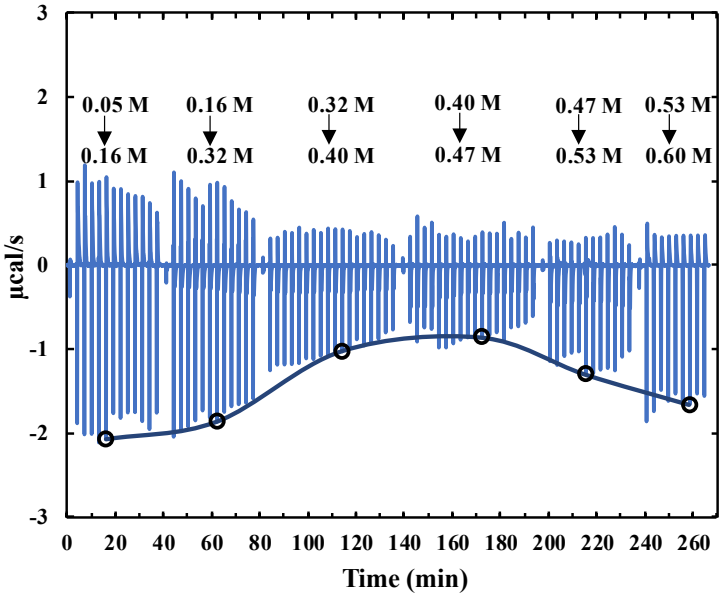
0.05 M
0.16 M
0.16 M
0.32 M
0.32 M
0.40 M
0.40 M
0.47 M
0.47 M
0.53 M
0.53 M
0.60 M
µcal/s
Time (min)

Figure 11

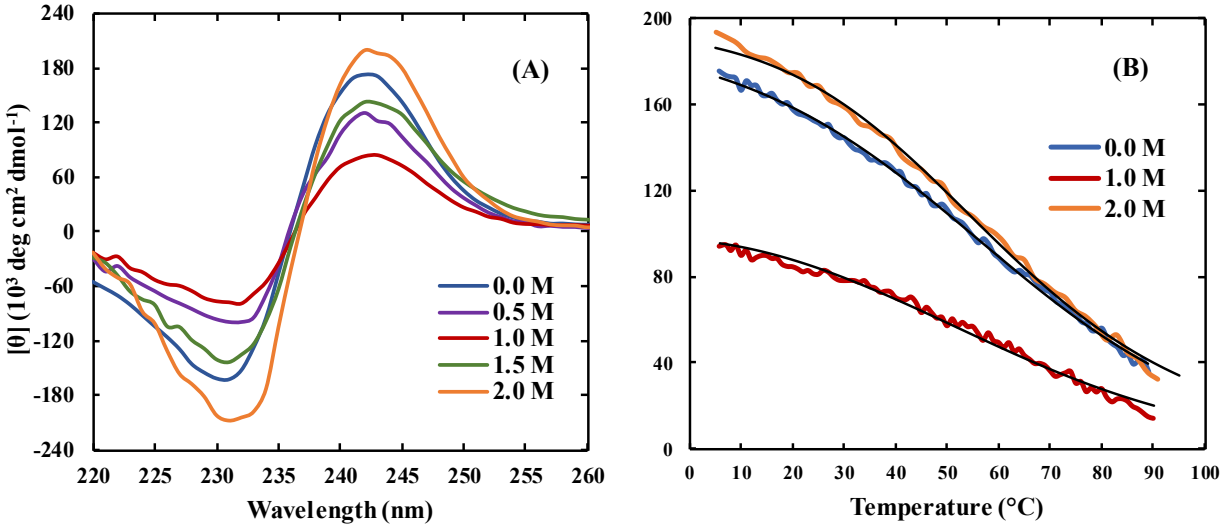
(A)
[θ] (10³ deg cm² dmol⁻¹)
Wavelength (nm)
0.0 M
0.5 M
1.0 M
1.5 M
2.0 M
(B)
Temperature (°C)
0.0 M
1.0 M
2.0 M

Figure 12

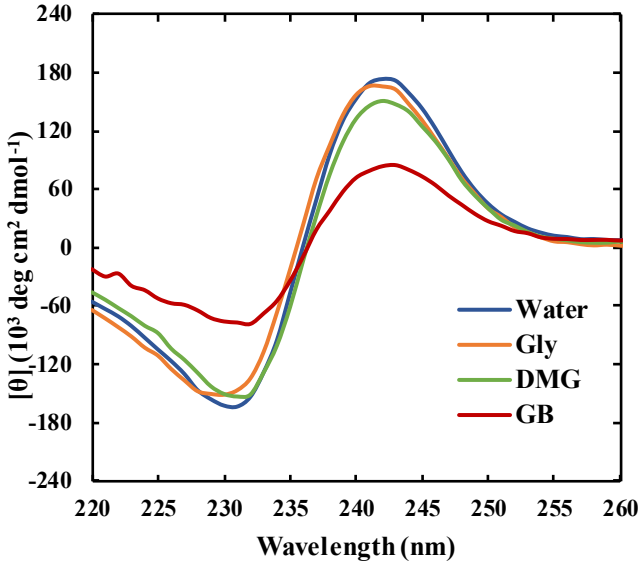
240
180
120
60
0
-60
-120
-180
-240
220
225
230
235
240
245
250
255
260
[θ]λ(10³ deg cm² dmol⁻¹)
Wavelength (nm)
Water
Gly
DMG
GB

TOC Figure